

$K_2AgInCl_6$: A promising material for optoelectronic and thermoelectric applications

S. M. Benchikh^a, M. Matougui^a, A. Messaoudi^a, B. Bouadjemi^a, A. Khatar^a,
S. Haid^{a,b}, H. Bentahar^a, M. Houari^{a,c}, T. Lantri^{a,c}, and S. Bentata^a

^aLaboratory of Technology and of Solids Properties, Abdelhamid Ibn Badis University, Mostaganem 27000, Algeria.
e-mail: matouguimohamed@hotmail.com

^bFaculty of Sciences and Technology, Tissemsilt University, 38000, Algeria.

^cUniversity of Relizane, Relizane, 48000, Algeria.

Received 7 October 2024; accepted 22 January 2025

Using the FP-LAPW method with the exchange and correlation potentials of the GGA and mBJ-GGA approximations, we have studied the structural, electronic, thermoelectric, and optical properties of the double perovskite halide compound $K_2AgInCl_6$. Our results indicate that this compound is stable in the nonmagnetic phase and exhibits structural stability according to the normative values of the Goldsmith factor (t) and octahedral factor (μ). It is thermodynamically stable, as evidenced by a negative formation energy. $K_2AgInCl_6$ acts as a semiconductor, displaying a direct band gap of 1.162 eV in GGA and 2.944 eV in mBJ-GGA. Thermoelectric analysis reveals excellent properties, with ZT values close to unity. However, the GGA approximation performs well at medium and high temperatures (300-800 K), while mBJ-GGA is more efficient at lower temperatures (50-100 K), with ZTs ranging from 0.73 to 0.7 for the latter approximation. In addition, $K_2AgInCl_6$ shows transparency in the infrared and visible spectrums, as well as strong absorption and reflectivity in the UV spectrum, making it suitable for various applications, including in broadband solar cells to improve efficiency through extended absorption. In optoelectronics, it can serve as a UV light emitter in high-power LEDs and potentially as a UV filter to protect materials and people from harmful radiation.

Keywords: FP-LAPW; double perovskite; semiconductor; goldschmidt factor; figure of merit ZT; optoelectronics.

DOI: <https://doi.org/10.31349/RevMexFis.71.040502>

1. Introduction

Halide perovskites, a group of inorganic materials with the formula ABX_3 , have seen rapid growth in materials science in recent years [1-3]. Their distinctive crystal structure, featuring an octahedral arrangement of BX_6 cations around A anions, gives them exceptional physical and chemical properties, making them promising for various applications. Among halide perovskites, double perovskites (DP) hold a special position. These materials, with the formula $A_2B_2X_6$, stand out for their two-dimensional structure, where layers of $[BX_6]^{n-}$ perovskites alternate with layers of A^{2+} cations. This unique design leads to novel electronic, optical, and magnetic properties, offering new possibilities in different research fields.

The appeal of double perovskites lies in their potential use in solar cells, optoelectronic devices, catalysts, and magnetic materials [4-6]. Their broad bandgap, chemical stability, and dopability make them excellent candidates for high-efficiency solar cell production. Their controlled light emission capabilities make them promising for light-emitting diodes and lasers. Their catalytic activity in diverse chemical reactions creates opportunities for energy conversion and organic compound synthesis. Their distinct magnetic properties make them attractive for developing multifunctional magnetic materials.

Recent progress in synthesizing and characterizing double perovskites has addressed stability and large-scale pro-

duction challenges. Ongoing research is exploring new compositions and doping techniques to enhance their properties for specific applications. In this investigation, the structural, electronic, thermoelectric, and optical characteristics of double perovskite $K_2AgInCl_6$ were examined. This theoretical analysis relies on a full potential linearized augmented plane wave (FP-LAPW) method within the wien2k code, using density functional theory (DFT). The exchange-correlation potential is handled through two approximations: the generalized gradient approximation (GGA) and modified Becke-Johnson approximation (mBJ). The article is structured as follows: Section 2 outlines the computational approach, Sec. 3 presents the findings, and Sec. 4 offers the conclusions.

2. Computational details

The analysis in this study on $K_2AgInCl_6$ double halide perovskite was conducted using the Full Potential Linearized Augmented Plane Wave (FP-LAPW) via density functional theory (DFT) [7] within the Wien2k package [8]. The exchange-correlation potential was treated using the generalized gradient approximation (GGA-PBE) [9]. Additionally, the generalized gradient approximation with the Becke-Johnson modification modified by Tran-Blaha was used (TB-mBJ - GGA) to correctly appreciate the value of the gap [10-14].

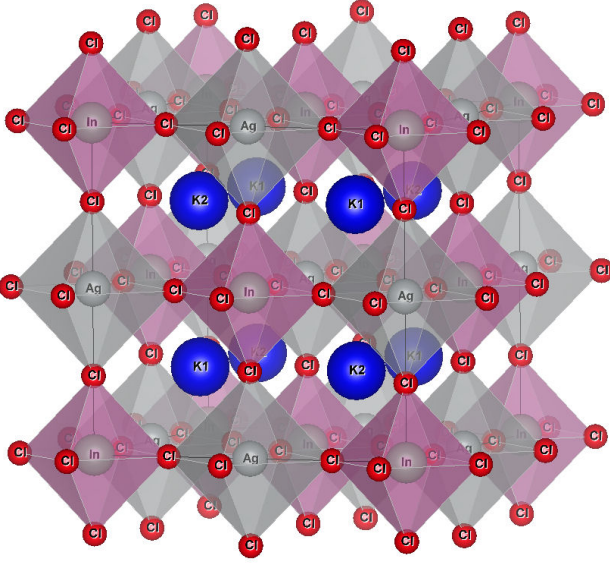


FIGURE 1. Crystal structure of cubic double perovskite $K_2AgInCl_6$.

This halide perovskite crystallizes in the cubic structure space group (Fm-3m, $n^\circ 225$) as shown in Fig. 1. In the FP-LAPW method, the space is divided into two regions: non-overlapping spheres surrounding the atomic sites of R_{MT} rays (Muffin-Tin) (Region I) and an interstitial region (Region II). In the calculations reported here, the radii of the muffin-tin (R_{MT}) spheres were chosen as 2.50, 2.50, 2.32, and 2.00 a.u. for K, Ag, In, and Cl, respectively. In Region I, the basic functions, electronic densities, and potentials are expanded using a combination of spherical harmonics up to $l_{max} = 10$ to ensure convergence of the eigenvalues. The extended charge density in Fourier space is taken up to $G_{max} = 14$. In Region II, the functions are treated as extended plane waves and expanded in a Fourier series with a cut-off parameter $R_{MT} \times K_{max} = 8$. This balance provides a trade-off between calculation accuracy and computational efficiency.

The $R_{MT} \times K_{max}$ parameter defines the size of the basis in the interstitial region, where R_{MT} is the smallest muffin-tin radius given in atomic units (a.u) and K_{max} represents the magnitude of the largest wave vector employed for developing the eigenfunctions in plane waves (wave vector cutoff for plane waves). The self-consistent calculation is considered converged when the total energy remains stable within 10^{-5} Ry. In addition, we conducted a self-consistent calculation using a $14 \times 14 \times 14$ -point mesh for structural and electronic properties calculations. Moreover, we employed a dense K-mesh of $30 \times 30 \times 30$ for optical properties calculations. Thermoelectric properties are calculated with a high density of 150000 k points utilizing the BoltzTraP code [15-17] in the Wien2k package. A relaxation time of 0.8×10^{-14} s is employed, following the guidance in the BoltzTraP user manual.

3. Results and discussions

3.1. Structural properties and stability

This section analyzes the materials in terms of structural and stability characteristics, which is essential to collect data on the molecular structure of the double halide perovskite $K_2AgInCl_6$, according to the principles of quantum mechanics. This allows predicting other properties, such as electronic, optical, and thermoelectric properties. Using the GGA approximation and the energy adjustment according to the cell volume, the results show that the paramagnetic (PM) phase has the lowest energy compared to the ferromagnetic (FM) phase. The total energy difference (ΔE) is calculated as follows:

$$\Delta E = E_{\text{stable phase}} - E_{\text{nearest phase}}. \quad (1)$$

So, the energy difference (ΔE) between the paramagnetic (PM) and ferromagnetic (FM) phase is calculated as follows: $\Delta E = E_{PM} - E_{FM}$. The obtained value is $\Delta E = -1.134 \times 10^{-2}$ eV, for the $K_2AgInCl_6$ material. The analysis examined the relationship between total energy and unit cell volume to obtain an appropriate fit using the Murnaghan equation of state [18]:

$$E(V) = E_0 + \frac{B}{B'}(B' - 1) \left[V \left(\frac{V_0}{V} \right)^{B'} - V_0 \right] + \frac{B}{B'}(V - V_0), \quad (2)$$

where $E(V)$ stands for the energy of the ground state when combined with cell volume V . Volume in the ground state is V_0 . The overall energy balance is E_0 . The bulk modulus and the derivative of pressure are denoted as B , B' , respectively.

Figure 2 shows how the total energy fluctuates for the strained $K_2AgInCl_6$ material as a function of the unit cell volume. By fitting the curves to the Murnaghan equation of

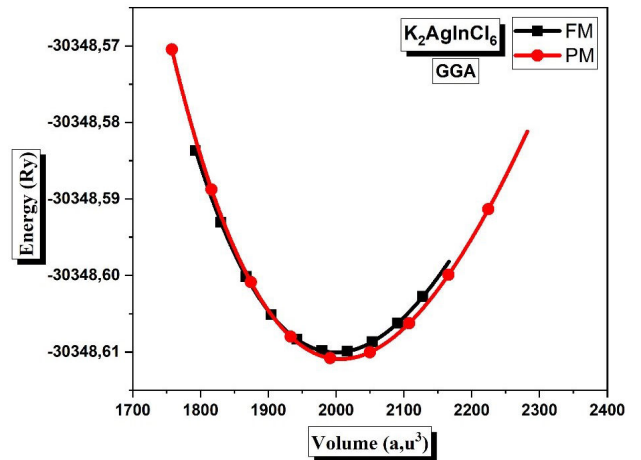


FIGURE 2. Total energy as a function of volume per formula unit for both ferromagnetic (FM), and non-magnetic (PM) states for the double perovskite $K_2AgInCl_6$.

TABLE I. Calculated equilibrium lattice parameter a_0 (Å), equilibrium energy E_0 (Ry), bulk modulus B (GPa), and its first derivative (B') for halide double perovskite K₂AgInCl₆ using GGA approximation for both states: ferromagnetic (FM) and paramagnetic (PM).

	V_o (Ry)	B (GPa)	BP	E_o (Ry)	a_o (Å)
FM	1999.3767	29.2161	4.8729	-30348.610054	10.5822
PM	2006.4150	29.4696	4.9107	-30348.610888	10.5952

state, the energy-volume curve of this compound in the paramagnetic arrangement exhibits a minimum energy clearly lower than that of the ferromagnetic phase, which indicates unequivocally that the halide double perovskite K₂AgInCl₆ is stable in the paramagnetic (or nonmagnetic) phase. On the other hand, the equilibrium lattice parameters, the bulk modulus, and its first pressure derivative of this material in this stability phase have been determined (see Table I). To ensure the stability of the double perovskite K₂AgInCl₆, it is essential to determine the Goldschmidt factor, given by the formula [19]:

$$t = \frac{2(r_K + r_{Cl})}{\sqrt{2} \left(\frac{r_{Ag} + r_{In}}{2} + r_{Cl} \right)}, \quad (3)$$

where r_K , r_{Cl} , r_{Ag} , and r_{In} are ionic radii in 6-coordinate octahedral arrangements for K, Cl, Ag, and In atoms, according to Shannon's table of effective ionic radii [20]. A Goldschmidt factor t close to 1 indicates a well-fitted perovskite structure, suggesting favorable crystal stability. In general, a t between 0.8 and 1.0 is considered favorable for the formation of stable perovskite structures. In our case, the calculation of the Goldschmidt factor for the double halide perovskite K₂AgInCl₆ gives the following result: $t = 0.843$. This value is close to the typical range (0.8 to 1.0) for stable perovskite structures, suggesting that K₂AgInCl₆ is likely to form a stable perovskite structure.

Another stability criterion for double perovskites is the octahedral factor μ . This factor is essential to evaluate the stability of double perovskite structures based on the geometric compatibility of the cations and anions forming the octahedron. In addition to the Goldschmidt factor, it allows predicting the existence of a perovskite structure without significant distortion. For halogenated double perovskites of general formula $A_2BB'X_6$, the octahedral factor must take into account the two types of metal cations B and B' (in our case, Ag and In). A common approach is to use an average value for these cations:

$$\mu_{Average} = \frac{r_{Ag} + r_{In}}{r_{Cl}}. \quad (4)$$

For a perovskite structure to be stable, the octahedral factor μ should generally be between 0.41 and 0.66. In this range, the octahedral structure (BX₆) formed by cations B and anions X is considered stable. Calculation of the octahedral factor μ for the double halide perovskite K₂AgInCl₆ gives the following result: $\mu_{Average} \approx 0.539$. This value is within the typical range (0.41 to 0.66) for stable octahedral

structures, suggesting that the K₂AgInCl₆ structure is geometrically stable from the octahedral arrangement point of view.

It is also important to calculate a key parameter to assess the thermodynamic stability of this material: the formation energy ΔH_f . This is crucial to predict the feasibility of synthesis, long-term stability, and functional properties of double perovskites. This calculation uses the following equation:

$$\Delta H_f = E_f^{K_2AgInCl_6} = E_{tot}^{K_2AgInCl_6} - (2E_K + E_{Ag} + E_{In} + 6E_{Cl}), \quad (5)$$

where $E_{tot}^{K_2AgInCl_6}$ is the total energy of the double perovskite K₂AgInCl₆, and E_K , E_{Ag} , E_{In} , and E_{Cl} are the atomic energies of the cations K⁺, Ag⁺, In³⁺, and anions Cl⁻, respectively.

A negative formation energy indicates that the formation of the perovskite structure is thermodynamically favorable. The more negative this value, the more stable the structure is relative to its constituent elements, meaning the material is less likely to spontaneously decompose. Calculation of the formation energy for the double halide perovskite K₂AgInCl₆ gives the following result:

$$E_f^{K_2AgInCl_6} = -1.67 \text{ eV/atom}. \quad (6)$$

The negative formation energy indicates that the synthesis of K₂AgInCl₆ from its elements is thermodynamically favorable and experimentally feasible.

3.2. Electronic properties: Band structure and density of states

Band structure is a key concept in solid-state physics, describing the relationship between electron energy, represented by quantized electron orbitals, and their wave vector in a crystalline material. It provides essential information about the optical and thermoelectric properties of the material. Band structure calculations for the nonmagnetic state, using the GGA-PBE and mBJ-GGA methods, are shown in Fig. 3, with the Fermi level set at 0 eV. The band structures show that the valence band maximum and the conduction band minimum are aligned along the symmetry axis for K₂AgInCl₆, indicating that this compound is a direct bandgap semiconductor. The double perovskite K₂AgInCl₆ exhibits bandgap values of 1.162 eV and 2.944 eV for the GGA and mBJ-GGA approximations, respectively (Table II). Both approaches indicate that the double perovskite K₂AgInCl₆ demonstrates

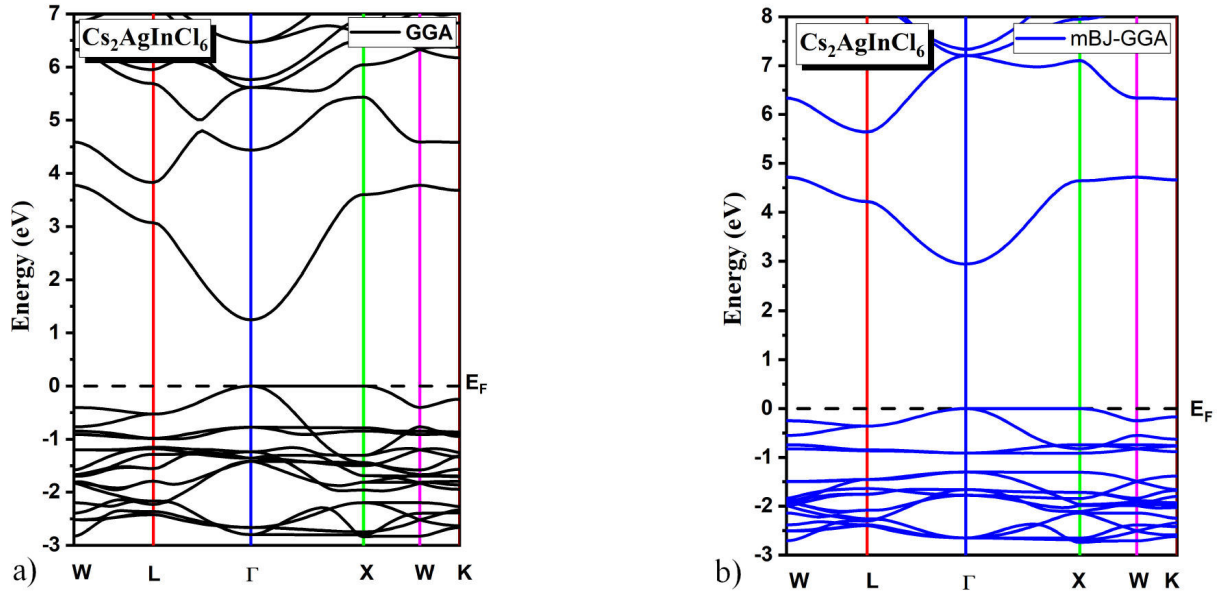


FIGURE 3. Band structures of $K_2AgInCl_6$ compound using GGA and mBJ GGA approximations.

TABLE II. Calculated values of energy gap (E_g) for halide double perovskite $K_2AgInCl_6$ using GGA and mBJ-GGA approximations.

E_g (eV)	GGA	mBJ-GGA
	1.162	2.944

semiconductor behavior. The main difference lies in the band gap value, with the mBJ-GGA method showing a larger band gap compared to the GGA method.

To understand the energetic contribution of the orbitals of the atoms of the compound in the valence and conduction bands, as well as to better understand the properties of the material and highlight its characteristics, the analysis of the total (TDOS) and partial (PDOS) orbitals is essential. The total and partial densities of states (TDOS and PDOS) of the studied materials were calculated by the GGA and mBJ-GGA methods, shown in Fig. 4, with the Fermi level (E_F) indicated by a vertical dashed line (0 eV). The results of both approaches are similar. The valence band of $K_2AgInCl_6$ is mainly dominated by the ($d, d_{-2} t_g$) states of Ag, close to the Fermi level, and by a minor contribution from the P states of Cl. The conduction band results mainly from the hybridization of the S orbitals of In and the P states of Cl, although the latter is not very significant. The presence of chlorine atoms around the Ag and In sites in $K_2AgInCl_6$ results in a doubling of the levels, creating a doubly degenerate state for the In atom (d and $d_{-2} t_g$), a strong hybridization of the doubly degenerate In states with the P orbitals of the Cl atoms is at the origin of the Gap.

3.3. Transport properties

The field of thermoelectric (TE) materials has gained importance in the last decade due to its potential in addressing the

energy crisis. Compounds with favorable TE properties hold promise in enhancing thermal technologies, energy production, refrigeration, and converting waste heat into electricity [21,22]. Researchers are driven to discover materials with low thermal conductivity akin to glass and high electrical conductivity like crystals. Developing high-efficiency thermoelectric materials is a significant challenge to meet market demands. The transport properties of the double perovskite compound $K_2AgInCl_6$ were analysed using Boltzmann transport theory and the theory of rigid bands via the BoltzTraP code in the Wien2k program. To describe the thermoelectric behavior of the halide double perovskite material $K_2AgInCl_6$, it is valuable to monitor how key parameters change with temperature. These parameters include electrical conductivity per relaxation time (σ/τ), the Seebeck coefficient (S), electronic thermal conductivity by relaxation time (k_e/τ), and the figure of merit (ZT). The variations of these parameters for $K_2AgInCl_6$ are illustrated in Fig. 4a) for the Seebeck coefficient (S); in Fig. 4b) for the electrical conductivity by relaxation time (σ/τ); in Fig. 4c) for the electronic thermal conductivity by relaxation time (k_e/τ); and finally in Fig. 4d) for the figure of merit ZT under the GGA and mBJ-GGA approximations. However, materials ideal for thermoelectric use require a high Seebeck coefficient, elevated electrical conductivity, reduced thermal conductivity, and a figure of merit near or above unity [23-26]. The transport characteristics of $K_2AgInCl_6$ were analyzed utilizing the BoltzTraP code [27] within the Wien2k software. The relaxation time constant τ , approximated at 0.8×10^{-14} s in accordance with the BoltzTraP user manual, was employed for calculations. Moreover, in this study, all the mentioned thermoelectric parameters were investigated within the temperature range of 0 to 900 K.

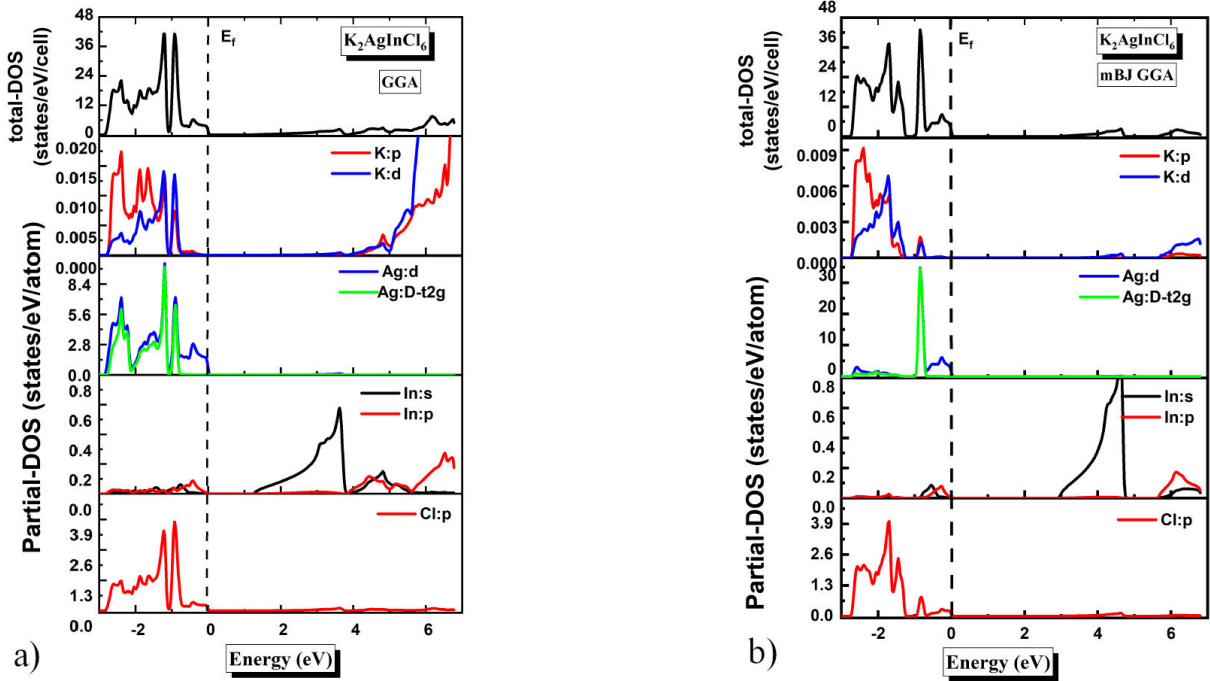


FIGURE 4. Calculated total (TDOS) and partial (PDOS) densities of states for halide double perovskites K₂AgInCl₆ using GGA and mBJ-GGA approximations. The Fermi energy is aligned to zero.

The Seebeck effect is a phenomenon where a potential difference appears at the junction of two materials under a temperature difference. This difference is due to the movement of free electrons from the hot zone to the cold zone. In materials where charge transport occurs with dominant positive charges (p-type), the Seebeck coefficient is positive, while for materials where charge transport occurs predominantly with electrons (n-type), it is negative. Materials with a high Seebeck coefficient are essential for efficient thermoelectric generators and coolers. For optimal performance, a material must have a high Seebeck coefficient. Figure 4a) illustrates the variability of the Seebeck coefficient S as a function of temperature for the double perovskite material K₂AgInCl₆. Let us first note the high values of the Seebeck coefficient for the two approximations (GGA and mBJ-GGA). According to this graphical representation, the Seebeck coefficient decreases with temperature, going from a maximum value of 247.9 $\mu\text{V/K}$ (50 K) to a minimum value of 171.8 $\mu\text{V/K}$ (800 K) for the mBJ-GGA approximation. While for the GGA approximation, the Seebeck coefficient initially increases up to a certain threshold (246.29 $\mu\text{V/K}$ at 200 K), then gradually decreases from this threshold to reach the minimum value of 185.36 $\mu\text{V/K}$ (800 K). The values of the Seebeck coefficients for the two approximations of this material are quite high, which is promising for thermoelectric applications, particularly at room temperature (300 K), with respective values of 203.8 $\mu\text{V/K}$ and 235.33 $\mu\text{V/K}$ according to the mBJ-GGA and GGA approximations. Furthermore, the S values obtained remain positive over the entire temperature range, suggesting the presence of P-type charge carriers (holes) as the main carriers. Electrical conductivity

measures a material's ability to conduct electrical charges. It contrasts with resistivity, which hinders charge movement by opposing it. Therefore, electrical conductivity, determined by relaxation time (σ/τ), showcases the interaction between free charge carriers (holes/electrons) and electric current. In thermoelectric applications, high electrical conductivity by relaxation time (σ/τ) is crucial for minimizing energy losses due to the Joule effect. The variation of electrical conductivity by relaxation time with temperature for this material is shown in Fig. 4b). According to the two approximations mentioned above, the curves appear quite similar. A significant increase in electrical conductivity (σ/τ) with temperature is clearly observed, with the charge carriers gaining mobility as the temperature increases considerably. The maximum values of (σ/τ) for the material K₂AgInCl₆ are: $13.62 \times 10^{18} [\Omega \cdot \text{m} \cdot \text{s}]^{-1}$ (800 K) and $16.28 \times 10^{18} [\Omega \cdot \text{m} \cdot \text{s}]^{-1}$ (800 K) for the approximations: mBJ-GGA and GGA, respectively. A narrower band gap increases the carrier concentration. Additionally, the low value of the effective masses of the charge carriers, linked to the quasi-parabolic shape of the electronic bands of the valence band, enhances carrier mobility, resulting in higher electrical conductivity. These findings point to significantly high electrical conductivity and, thus, low resistivity for the material. This property allows for the transport of electrical charges with minimal Joule effect losses, making it a promising thermoelectric material.

Thermal conductivity is a crucial factor in optimizing thermoelectric materials. Lowering thermal conductivity without compromising electrical conductivity is key. In semiconductor materials, thermal conductivity K comes from both electron (K_e) and phonon (K_l) contributions, where

$K = K_e + K_l$. To enhance thermoelectric materials, reducing the lattice vibrations contribution is essential, rather than the charge carriers' contribution.

Figure 4c) depicts the evolution of electronic thermal conductivity by relaxation time (K_e/τ) versus temperature for the material $K_2AgInCl_6$ based on the two aforementioned approximations. These curves indicate an increase in thermal conductivity with rising temperature for the material under study. It is noteworthy that the plots for electrical conductivity and electronic thermal conductivity exhibit a striking resemblance. These findings align with the Wiedemann-Franz law, which posits a direct relationship between these parameters:

$$K_e = \sigma LT \quad [28],$$

where L represents the Lorenz number, σ denotes electrical conductivity, and T stands for absolute temperature. The electronic thermal conductivity values hover around 1.56×10^{14} [W/m.K.s] and 1.12×10^{14} [W/m.K.s] at room temperature ($T = 300$ K) for the mBJ, GGA and GGA approximations, respectively. The characteristics of a thermoelectric

material are evaluated by a dimensionless parameter, known as the figure of merit ZT , defined by the equation:

$$ZT = \frac{S^2 T \sigma}{K}.$$

With T being the absolute temperature (in Kelvin), S representing the Seebeck coefficient (or thermoelectric power), σ denoting the electrical conductivity, and K standing for the thermal conductivity. To maximize the transport properties of a material, the figure of merit ZT must be high (close to or greater than unity). This requires that the Seebeck coefficient S and the electrical conductivity σ be maximized, while minimizing the thermal conductivity K without compromising electronic charge transport.

Figure 4d) illustrates the evolution of the figure of merit (ZT) as a function of temperature T . According to the mBJ-GGA approximation, we observe a decrease in this factor with increasing temperature, going from 0.73 (50 K) to 0.68 (800 K). On the other hand, for the GGA approximation, the figure of merit increases from 0.66 (50 K) to 0.73 (800 K). The ZT values are quite close to unity, making them very at-

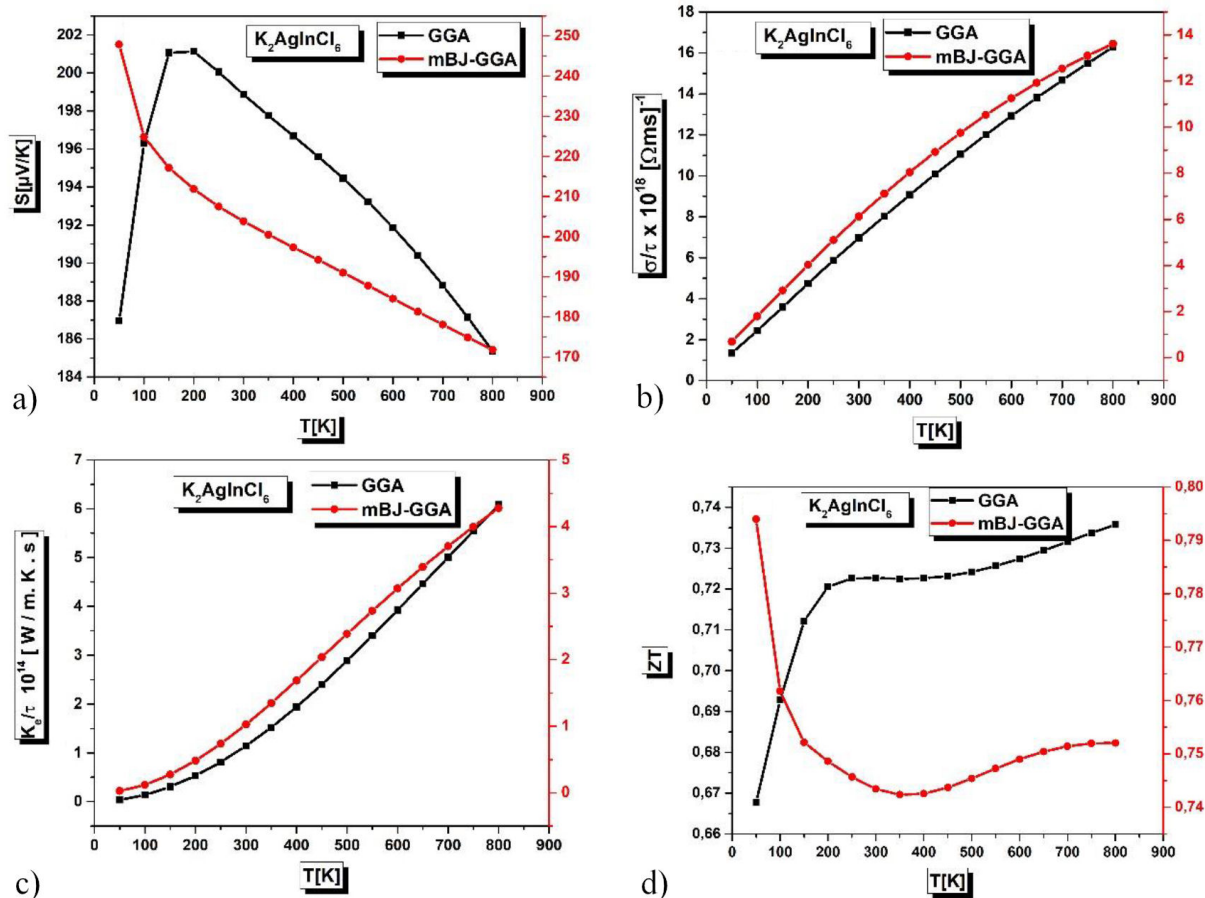


FIGURE 5. Thermoelectric properties calculated as a function of temperature for the double perovskite $K_2AgInCl_6$ using GGA and mBJ-GGA approximations for: a) Seebeck coefficient (S), b) electric conductivity per relaxation time (σ/τ), c) electronic thermal conductivity per relaxation time (k_e/τ) and d) merit factor (ZT).

TABLE III. Calculated different thermoelectric parameters at 300 K and maximum values: Seebeck coefficient S ($\mu\text{V/K}$), electrical conductivity per relaxation time σ/τ ($\times 10^{18}$ [Ωms]⁻¹), electronic conductivity per relaxation time K_e/τ ($\times 10^{14}$ [$\text{W/m}\cdot\text{K}\cdot\text{s}$]) and figure of merit (ZT) for halide double perovskite K₂AgInCl₆ using GGA and mBJ-GGA approximations.

	At 300K				Maximum values			
	ZT	k_e/τ	S	σ/τ	ZT	k_e/τ	S	σ/τ
GGA	0.73	1.12	235.33	6.89	0.73	6.06	245.73	16.28
mBJ-GGA	0.67	1.56	203.8	8.05	0.73	4.24	247.90	13.58

tractive for thermoelectric applications. At room temperature (300 K), the figure of merit is 0.73 for the GGA approximation. The double perovskite material K₂AgInCl₆ thus exhibits excellent thermoelectric properties due to its significant figure of merit. According to the GGA approximation, this material is thermoelectrically efficient for medium and high temperatures [300-800 K]. In this temperature range, the figure of merit is approximately 0.73. On the other hand, according to the mBJ-GGA approximation, the thermoelectric efficiency is felt over the low temperature range [50-100 K], with a figure of merit ZT fluctuating between 0.73 and 0.7. By favoring the mBJ-GGA approach, which in my opinion is the most appropriate for the study of this material, the double perovskite material K₂AgInCl₆ presents high thermoelectric efficiency but confined in the low temperature range. Table III presents the values of thermoelectric parameters of the K₂AgInCl₆ material at 300 K, along with their maximum values. The parameters include the Seebeck coefficient (S), electrical conductivity by relaxation time (σ/τ), electronic thermal conductivity by relaxation time (K_e/τ), and figure of merit (ZT). These elements are essential for evaluating the thermoelectric response of materials and their potential in thermoelectric devices. No experimental study has yet been carried out on this material, so it would be very useful to conduct one to confirm these results.

3.4. Optical properties

The optical properties of double perovskite materials are crucial for various photovoltaic applications, including light-emitting diodes (LEDs), light detectors, and other optoelectronic devices, by exploiting the photovoltaic effect. In particular, the absorption and emission of light directly influence the efficiency of these materials as photovoltaics. Optimizing these properties is essential to improve the conversion of solar energy into electricity, thus promoting the development of high-efficiency solar cells. Since the double halide perovskite K₂AgInCl₆ is a direct gap material according to both GGA and mBJ-GGA approximations, it would be much more interesting to evaluate the optical properties of this material. In a direct gap material, electrons jump directly from the valence band to the conduction band when excited by a photon, which allows them to absorb and emit light more efficiently. This makes the material even more effective for optoelectronic devices such as light-emitting diodes (LEDs) and semiconduc-

tor lasers, which rely on direct gap materials to emit light efficiently.

To attain this, we perform calculations of the optical properties of K₂AgInCl₆ with the mBJ-GGA approximation. To measure the linear response in this study, we use the complex dielectric function $\varepsilon(\omega)$, which can be expressed as [29-32]:

$$\varepsilon(\omega) = \varepsilon_1(\omega) + i\varepsilon_2(\omega),$$

where $\varepsilon_1(\omega)$ and $\varepsilon_2(\omega)$ represent the real and imaginary parts of the dielectric function, respectively, with ω denoting the angular frequency of the incident radiation.

This study examines the optical properties-specifically, the dielectric function, absorption, and reflectivity-of the double-halide perovskite K₂AgInCl₆ for photon energies ranging from 0 to 15 eV, as shown in Fig. 6. The real part of the dielectric function $\varepsilon_1(\omega)$ determines a material's refractive and reflective index, which influences how light is refracted or reflected at its surface. In optical devices such as mirrors and lenses, controlling these properties is essential to manage the direction (polarization) and intensity of light.

Figure 6a) illustrates the fluctuations of the real part of the dielectric function $\varepsilon_1(\omega)$ as a function of the energy of the incident radiation. First, let us note that $\varepsilon_1(0)$, the static permittivity of the material, is equal to 2.8. This value represents the ability of the material to polarize in response to a static electric field. This value is relatively modest, meaning that the material has a significant polarization ability, but not as high as some other materials. This suggests that the material is neither highly polarizable nor weakly polarizable, and is typical of some semiconductors [33-35] with a moderate gap, where the valence electrons are not too strongly bound, allowing some electronic polarization. The values of $\varepsilon_1(\omega)$ decrease, following a succession of peaks, to reach negative values, in the energy range 10-14 eV (*i.e.* the UV region), which implies a strong reflection of light in this energy range, since the material acts as a mirror for these wavelengths. This can lead to specific absorption at certain frequencies, which is useful for designing optical filters or selective absorbers. Moreover, one of the striking consequences of negative permittivity is the possibility of negative refraction, which means that light refracts in a direction opposite to that expected in classical materials.

The imaginary part of the dielectric function, $\varepsilon_2(\omega)$, is related to the absorption of energy by the material under an electromagnetic field, caused by the radiation of the incident

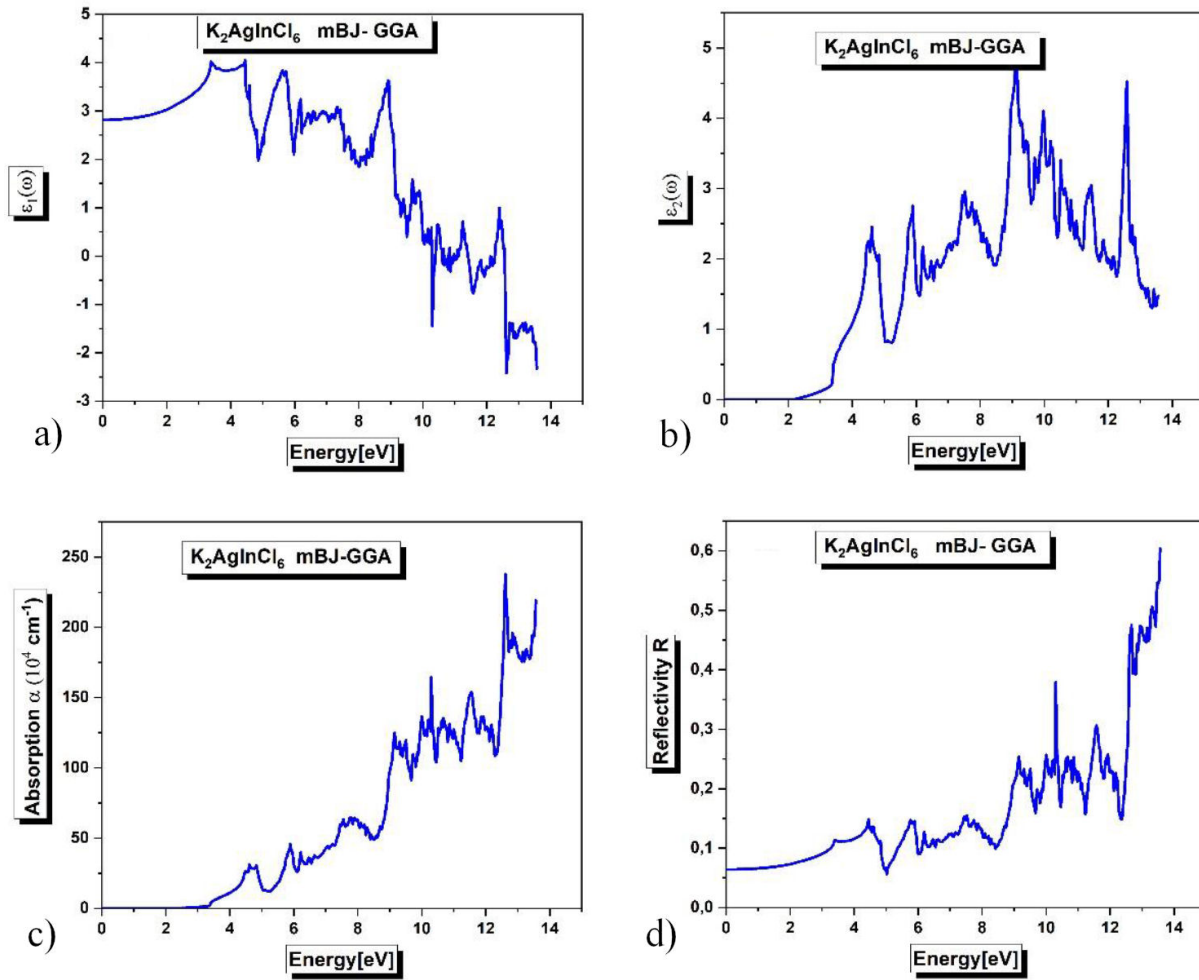


FIGURE 6. The real $\epsilon_1(\omega)$ a) and imaginary $\epsilon_2(\omega)$ b) part of the dielectric function, the absorption α c) and the reflectivity R d) for double halide perovskite $K_2AgInCl_6$, calculated by mBJ-GGA approximation.

wave. This corresponds to electronic transitions between the valence and conduction bands. It is essential for understanding the interaction of a material with light, its optical properties (transparency and opacity), and its use in applications such as optical filters, absorbers, and photovoltaic devices. Figure 6b) shows the imaginary part of the dielectric function $\epsilon_2(\omega)$ for $K_2AgInCl_6$.

An important feature of the imaginary part of the dielectric function $\epsilon_2(\omega)$ is its minimum threshold, which can be interpreted as the point where the absorption starts to increase significantly. This minimum threshold defines the beginning of the region where the material starts to interact significantly with electromagnetic radiation. In semiconductors, this is often close to the band gap energy E_g . In the present case, the minimum threshold of the double halide perovskite compound $K_2AgInCl_6$ is equal to 2.84 eV (*i.e.*, in the visible spectrum region), which is close to the gap energy E_g (2.94 eV, see Table II).

Just after the photon energy reaches E_g , the minimum energy required to excite an electron from the valence band to the conduction band, a succession of peaks follows. Each

peak in $\epsilon_2(\omega)$ corresponds to a particular electronic transition where electrons are excited from a lower energy state to a higher one. For semiconductors, this usually involves transitions from the valence band to the conduction band. These peaks indicate the energies where the material absorbs or emits efficiently, which is crucial for optoelectronic devices.

The $K_2AgInCl_6$ material having a minimum threshold of $\epsilon_2(\omega)$ in the visible spectrum suggests that the material may be relatively transparent in the visible spectrum, as it does not significantly absorb visible light. However, the ensuing succession of peaks appearing in the UV region suggests a strong absorption in the UV, making this material suitable for UV protection applications, such as UV filters, or in devices that exploit UV absorption for electricity generation, such as broad-spectrum solar cells.

Optical absorption is a key process in optics and materials physics, where a material absorbs some of the light energy passing through it, thereby reducing the intensity of the transmitted light. Optical absorption is crucial for the operation of optoelectronic devices such as solar cells, photode-

tectors, and LEDs. In solar cells, the efficiency of converting light into electricity depends on the ability of the material to absorb light from the solar spectrum. Figure 6c) illustrates the absorption coefficients of K₂AgInCl₆ versus photon energy using the mBJ-GGA approximation. The fundamental absorption threshold starts at 2.87 eV for K₂AgInCl₆, which roughly corresponds to the band gap E_g of this semiconductor material, defining the minimum energy required for significant electronic absorption. Below this threshold, the absorption coefficient is practically zero. This implies that this compound does not significantly absorb radiation in the IR and visible spectrum; however, it exhibits significant absorption over a wide range of photon energies in the UV spectrum, demonstrating the usefulness of this compound for various optical and optoelectronic devices operating in this UV spectral range, such as solar cells or photovoltaic cells.

For the double perovskite (DP) K₂AgInCl₆, the maximum absorption coefficient ($237.78 \times 10^4 \text{ cm}^{-1}$) is reached when the photon energy reaches 12.61 eV (UV radiation). Reflectivity measures the amount of incident light reflected by the surface of a material, without absorption or penetration. In optics, for a semiconductor, reflectivity is an essential property related to the intrinsic characteristics of the material. In Fig. 6d), we have the plot of the reflectivity variations $R(\omega)$ of K₂AgInCl₆.

Let us first note the value of $R(0)$, which represents the zero-energy reflectivity of the material, also called computed static reflectivity; physically, this situation corresponds to an electromagnetic wave of very long wavelength (because the energy of a photon is inversely proportional to its wavelength). In the case of this study, $R(0) = 6.49\%$. Comparing the plot of the curves of the real part of the dielectric function $\varepsilon_1(\omega)$ [Fig. 6a)] and that of the reflectivity $R(\omega)$ [Fig. 6d)], it should be noted that the high values of $R(\omega)$ occur when the real part of the dielectric constant $\varepsilon_1(\omega)$ has negative values. Furthermore, by observing the reflectivity spectrum, it is clear that this compound exhibits a strong reflection in energies above 10 eV, corresponding to ultraviolet radiation.

The maximum reflectivity recorded is 60.42% for a photon energy of 13.56 eV (UV radiation). This property of dominant reflectivity in the UV makes it advantageous for UV devices and applications. Their ability to efficiently reflect UV radiation can be valuable in various technological applications, such as UV sensors, photodetectors, and other optoelectronic devices operating in the UV spectrum.

In conclusion, the double perovskite (DP) material K₂AgInCl₆, characterized by transparency in the infrared and visible regions, coupled with strong absorption and reflectivity in the ultraviolet, opens many application perspectives, such as broadband solar cells. This is due to its ability to absorb UV, which extends the absorption spectrum of solar

cells, thus increasing their efficiency. Similarly, it can be used in optoelectronics as a UV light emitter in high-power LEDs, as it could find its use as a UV filter, thanks to its strong absorption in the UV, thus protecting materials and people from the harmful effects of ultraviolet rays.

4. Conclusion

In conclusion, using the Full Potential Linearized Augmented Plane Wave (FP-LAPW) method and the exchange and correlation potentials of the following approximations: the generalized gradient approximation (GGA) and the modified Becke-Johnson generalized gradient approximation (mBJ-GGA), we have performed a theoretical analysis to calculate the structural, electronic, thermoelectric, and optical properties of the double perovskite halide compound K₂AgInCl₆. The results of the study indicate that the investigated compound exhibits stability in the non-magnetic phase. Furthermore, it is characterized by structural stability, following the normative values of both the Goldsmith factor t and the octahedral factor μ , and is thermodynamically stable and experimentally realizable due to the negative value of the formation energy.

Moreover, this material exhibits semiconductor behavior with a direct band gap of 1.162 eV in GGA and 2.944 eV in mBJ-GGA, according to its electronic properties. Thermoelectric parameter analysis reveals that the K₂AgInCl₆ double perovskite material has excellent properties, with ZT values close to unity. The GGA approximation indicates its efficiency at medium and high temperatures (300-800 K), while the mBJ-GGA approximation shows its efficiency at low temperatures (50-100 K), with a ZT figure of merit ranging from 0.73 to 0.7.

Due to its optical properties, the double perovskite (DP) material K₂AgInCl₆, due to its transparency in the infrared and visible spectra, as well as its high absorption and reflectivity in the UV, offers many applications, especially in broadband solar cells, where it increases efficiency by broadening the absorption spectrum. It can also be used in optoelectronics as a UV light emitter in high-power LEDs, as it could be the main substance of a UV filter, thus protecting materials and people from the harmful effects of ultraviolet rays.

Given the lack of experimental data on the K₂AgInCl₆ double perovskite material, our theoretical predictions regarding its structural, electronic, optical, and thermoelectric properties are likely to be experimentally validated. Thus, our study represents a prospective exploration of this promising material for applications in optoelectronics and thermoelectrics, particularly in the UV range, with a figure of merit ZT close to unity.

1. F. Estrada Chávez, E. J. Guzmán, B. Aguilar, O. Navarro, and M. Avignon, Increase of Curie temperature with La doping in the double perovskite Sr₂-LaFeMoO₆ within an electronic correlation approach, *Rev. Mex. Fis.* **64** (2018) 145, <https://doi.org/10.31349/RevMexFis.64.145>
2. Y. Bouchentouf Idriss, Hubbard's parameter influence on Ba₂GdReO₆ properties, a promising ferromagnetic double Pérovskite oxide for thermoelectric applications, *Rev. Mex. Fis.* **69** (2023) 051006. <https://doi.org/10.31349/RevMexFis.69.051006>
3. L. F. Blaha, A. Maafa, A. Chahed, M. Boukli, and A. Sayade, The first principle calculations of structural, magneto-electronic, elastic, mechanical, and thermoelectric properties of half-metallic double perovskite oxide Sr₂TiCoO₆, *Rev. Mex. Fis.* **67** (2021) 114, <https://doi.org/10.31349/RevMexFis.67.114>
4. A. M. Reyes, Y. Arredondo, and O. Navarro, First principles study of the effects of disorder in the Sr₂FeMoO₆ perovskite, *Rev. Mex. Fis.* **62** (2016) 160.
5. A. Labdelli, and N. Hamdad, Predictive study of ferromagnetism and antiferromagnetism coexistence in Ba_{1-x}Gd_xRuO₃ induced by Gd-doping, *Rev. Mex. Fis.* **67** (2021) 061002, <https://doi.org/10.31349/RevMexFis.67.061002>
6. A. Lemziouka, F. Nekkach, H. Lemziouka, R. Moubah, A. Boutahar, M. El Yazidi, and M. Lamiae, Investigation of the structural and optical characteristics of La₂FeCrO₆ double perovskite for optoelectronic applications, *Journal of Molecular Structure*, **1316** (2024) 138884, <https://doi.org/10.1016/j.molstruc.2024.138884>
7. P. Blaha, K. Schwarz, G. K. Madsen, D. Kvasnicka, and J. Luitz, "wien2k", An augmented plane wave+ local orbitals program for calculating crystal properties, (2001).
8. M. Houari, B. Bouadjemi, A. Abbad, W. Benstaali, S. Haid, and T. Lantri, Structural, electronic and optical properties of cubic fluoroelpasolite Cs₂NaYF₆ by density functional theory, *Chinese Journal of Physics*, **56** (2018) 1756, <https://doi.org/10.1016/j.cjph.2018.05.004>.
9. J. P. Perdew and K. Burke, and M. Ernzerhof, Generalized gradient approximation made simple, *Physical review letters*, **77** (1996) 3865, <https://doi.org/10.1103/PhysRevLett.77.3865>.
10. D. Koller, F. Tran, and P. Blaha, Merits and limits of the modified Becke-Johnson exchange potential, *Physical Review B*, **83** (2011) 195134, <https://doi.org/10.1103/PhysRevB.83.195134>.
11. D. J. Singh, Electronic structure calculations with the Tran-Blaha modified Becke-Johnson density functional, *Physical Review B*, **82** (2010) 205102, <https://doi.org/10.1103/PhysRevB.82.205102>.
12. N. N. Anua, R. Ahmed, A. Shaari, M. A. Saeed, B. U. Haq, and S. Goumri-Said, Non-local exchange correlation functionals impact on the structural, electronic and optical properties of III-V arsenides, *Semiconductor Science and Technology*, **28** (2013) 105015, <https://doi.org/10.1088/0268-1242/28/10/105015>.
13. D. Behera, and S.K. Mukherjee, Mater first-principles calculations to investigate structural, optoelectronics and thermoelectric properties of lead free Cs₂GeSnX₆ (X = Cl, Br), *Sci. Eng. B* **292** (2023) 116421, <https://doi.org/10.1016/j.mseb.2023.116421>.
14. F. Tran and P. Blaha, Accurate band gaps of semiconductors and insulators with a semilocal exchange-correlation potential, *Physical review letters*, **102** (2009) 226401. <https://doi.org/10.1103/PhysRevLett.102.226401>.
15. M. Bilal, B. Khan, H. R. Aliabad, M. Maqbool, S. J. Asadabadi, and I. Ahmad, Thermoelectric properties of Sb-Na₃ and Bi-Na₃ for thermoelectric devices and alternative energy applications, *Computer Physics Communications*, **185** (2014) 1394, <https://doi.org/10.1016/j.cpc.2014.02.001>.
16. R. Bentata *et al.*, New p-type sp-based half-Heusler compounds LiBaX (X= Si, Ge) for spintronics and thermoelectricity via ab-initio calculations, *Journal of Computational Electronics*, **20** (2021) 1072, <https://doi.org/10.1007/s10825-021-01702-x>.
17. A. Mera, S. Awais Rouf, T. Zelai, N. A. Kattan and Q. Mahmood, Study of inorganic double perovskites Cs₂RbZl₆ (Z = Ga, In) as energy harvesting aspirant: a DFT approach, *Optical and Quantum Electronics*, (2023) <https://doi.org/10.1007/s11082-023-05195-9>
18. F. D. Murnaghan, The compressibility of media under extreme pressures. *Proc. Natl. Acad. Sci. USA* **30** (1944) 244, <https://doi.org/10.1073/pnas.30.9.244>.
19. J. B. Goodenough, J. M. Longo, and K. H. Hellwege, Crystallographic and Magnetic Properties of Perovskite and Perovskite-Related Compounds (Ed), Landolt-Bornstein Tabellen, New Series III 4a, (Springer-Verlag, Berlin, 1970) 126.
20. R.D. Shannon, Revised effective ionic radii and systematic studies of interatomic distances in halides and chalcogenides. *Acta Cryst. A* **32** (1976) 751, <https://doi.org/10.1107/S0567739476001551>.
21. S.A. Sofi, D.C. Gupta, Robustness in ferromagnetic phase stability, half-metallic behavior and transport properties of cobalt-based full-Heuslers compounds: A first principles approach. *Int J Quantum Chem.* **121** (2021) e26538. <https://doi.org/10.1002/qua.26538>
22. P.K. Kamlesh, R. Gautam, S. Kumari, and A.S. Verma, Investigation of inherent properties of XScZ (X = Li, Na, K; Z = C, Si, Ge) half-Heusler compounds: Appropriate for photovoltaic and thermoelectric applications, *Physica B: Physics of Condensed Matter* (2020), <https://doi.org/10.1016/j.physb.2020.412536>
23. S. Haid, W. Benstaali, A. Abbad, B. Bouadjemi, S. Bentata and Z. Aziz, Thermoelectric, Structural, Optoelectronic and Magnetic properties of double perovskite Sr₂CrTaO₆: First principle Study, *Materials Science & Engineering B* **245** (2019) 68, <https://doi.org/10.1016/j.mseb.2019.05.013>
24. B. Bouadjemi, T. Lantri, M. Matougui, M. Houari, R. Bentata, Z. Aziz and S. Bentata, High Spin Polarization and Thermoelectric Efficiency of Half-Metallic Ferromagnetic CrYSn (Y = Ca, Sr) of Half-Heusler Compounds, *SPIN*, **10** (2020) 2050010, <https://doi.org/10.1107/S0567739476001551>.

25. M. Matougui *et al.*, Rattling Heusler semiconductors' thermoelectric properties: First-principles prediction, *Chinese Journal of Physics*, **57** (2019) 195, <https://doi.org/10.1016/j.cjph.2018.11.015>.
26. M. Houari *et al.*, Semiconductor behavior of halide perovskites AGeX₃ (A= K, Rb and Cs; X= F, Cl and Br): first-principles calculations, *Indian J Phys* (2019) 1, <https://doi.org/10.1007/s11082-019-1949-y>.
27. G. K. Madsen and D.J. Singh, *Computer Physics Communications* **175** (2006) 67,
28. A. Bejan and A.D. Kraus, Heat transfer handbook, (John Wiley & Sons, 2003)
29. M. Houari *et al.*, Optoelectronic properties of germanium iodide perovskites AGeI₃ (A = K, Rb and Cs): first principles investigations, *Optical and Quantum Electronics*, **51** (2019) 234.
30. S. Haid, B. Bouadjemi, M. Houari, M. Matougui, T. Lantri, S. Bentata, and Z. Aziz. Optical properties of half-metallic ferromagnetic double perovskite Sr₂CaOsO₆ compound, *Solid State Communications* **322** (2020) 114052. <https://doi.org/10.1016/j.ssc.2020.114052>.
31. M. Houari *et al.*, Structural, electronic and optical properties of cubic fluoroelpasolite Cs₂NaYF₆ by density functional theory, *Chinese journal of physics*, **56** (2018) 1756, <https://doi.org/10.1016/j.cjph.2018.05.004>.
32. J. Nam Joong *et al.*, Compositional engineering of perovskite materials for high-performance solar cells, *Nature*, **517** (2015) 476, <https://doi.org/10.1038/nature14133>.
33. K. Sadia *et al.*, Utilizing density functional theory (DFT) approach for predicting the optoelectronic, structural, and magnetic properties of the spin-polarized scintillating bromo-elpasolite Cs₂LiCeBr₆, *Optical and Quantum Electronics*, **55** (2023) 861. <https://doi.org/10.1007/s11082-023-05122-y>.
34. K. Arvind, M. Kumar, and R.P. Singh, Magnetic, optoelectronic, and thermodynamic properties of half-metallic double perovskite oxide, Ba₂YbTaO₆: a density functional theory study, *Journal of Materials Science: Materials in Electronics*, **32** (2021) 12951, <https://doi.org/10.1007/s10854-021-05637-8>.
35. J. Sahariya, P. Kumar, and A. Soni, Structural and optical investigations of ZnGa₂X₄ (X= S, Se) compounds for solar photovoltaic applications, *Materials Chemistry and Physics*, **199** (2017) 257, <https://doi.org/10.1016/j.matchemphys.2017.07.003>.